communications earth & environment

ARTICLE

https://doi.org/10.1038/s43247-023-00991-3 OPEN

Space weathering acts strongly on the uppermost surface of Ryugu

Moe Matsuoka[1✉], Ei-ichi Kagawa[2], Kana Amano[2], Tomoki Nakamura[2], Eri Tatsumi[3,4], Takahito Osawa[5], Takahiro Hiroi[6], Ralph Milliken[6], Deborah Domingue[7], Driss Takir[8], Rosario Brunetto[9], Antonella Barucci[10], Kohei Kitazato[11], Seiji Sugita[4,12,13], Yuri Fujioka[2], Osamu Sasaki[14], Shiho Kobayashi[2], Takahiro Iwata[15,16], Tomokatsu Morota[4], Yasuhiro Yokota[15], Toru Kouyama[17], Rie Honda[18], Shingo Kameda[19], Yuichiro Cho[4], Kazuo Yoshioka[20], Hirotaka Sawada[15], Masahiko Hayakawa[15], Naoya Sakatani[15], Manabu Yamada[13], Hidehiko Suzuki[21], Chikatoshi Honda[11], Kazunori Ogawa[15], Kei Shirai[22], Cateline Lantz[9], Stefano Rubino[9], Hisayoshi Yurimoto[23], Takaaki Noguchi[24], Ryuji Okazaki[25], Hikaru Yabuta[26], Hiroshi Naraoka[25], Kanako Sakamoto[15], Shogo Tachibana[4,15], Toru Yada[15], Masahiro Nishimura[15], Aiko Nakato[15], Akiko Miyazaki[15], Kasumi Yogata[15], Masanao Abe[15,16], Tatsuaki Okada[15], Tomohiro Usui[15], Makoto Yoshikawa[15,16], Takanao Saiki[15,16], Satoshi Tanaka[15,16], Fuyuto Terui[27], Satoru Nakazawa[15], Sei-ichiro Watanabe[28] & Yuichi Tsuda[15]

Returned samples from Cb-type asteroid (162173) Ryugu exhibit very dark spectra in visible and near-infrared ranges, generally consistent with the Hayabusa2 observations. A critical difference is that a structural water absorption of hydrous silicates is around twice as deep in the returned samples compared with those of Ryugu's surface, suggesting Ryugu surface is more dehydrated. Here we use laboratory experiments data to indicate the spectral differences between returned samples and asteroid surface are best explained if Ryugu surface has (1) higher porosity, (2) larger particle size, and (3) more space-weathered condition, with the last being the most effective. On Ryugu, space weathering by micrometeoroid bombardments promoting dehydration seem to be more effective than that by solar-wind implantation. Extremely homogeneous spectra of the Ryugu's global surface is in contrast with the heterogeneous S-type asteroid (25143) Itokawa's spectra, which suggests space weathering has proceeded more rapidly on Cb-type asteroids than S-type asteroids.

A full list of author affiliations appears at the end of the paper.

The Japan Aerospace Exploration Agency's (JAXA's) Hayabusa2 spacecraft successfully returned material from asteroid (162173) Ryugu to Earth on 6 December 2020, and a series of initial analyses were conducted on select grains from the bulk material[1–4]. Ryugu is a near-Earth asteroid with a very low albedo (~4.7% of geometric albedo based on ground telescopic observations[5]) and is classified as type Cb or F in the C-complex asteroids[6,7]. C-complex asteroids are believed to be the parent bodies of carbonaceous chondrite meteorites based on their dark and flat spectral shape at visible (Vis: typically ~0.4–0.9 μm) and near-infrared (NIR: ~0.9–2.5 μm) wavelengths. Vis-NIR data acquired during the asteroid encounter by the Hayabusa2 Optical Navigation Camera (ONC-T) and near-infrared spectrometer (NIRS3) confirmed material on Ryugu is exceptionally dark, has experienced aqueous alteration as evidenced by the presence of structural water absorptions in hydrous silicates, and is spectrally consistent with hydrated carbonaceous chondrites[6,8]. Ryugu grains collected from the first touchdown (TD1) site and the second touchdown (TD2) site have been stored in Chambers A and C, respectively. The uppermost surface grains were captured at both TD1 and TD2 sites. Chamber C grains have been expected to include sub-surface-derived grains, excavated by small carry-on impactor (SCI) experiment producing a 1.7-m depth artificial crater on Ryugu[9]. Initial laboratory characterization of both Chambers A and C grains show that the material has experienced strong aqueous alteration, is most similar to CI (Ivuna-type) chondrites, and is representative of Ryugu's surface based on spectral and morphological properties[1,10,11]. The bulk elemental and isotopic analyses of Ryugu samples has also demonstrated that Ryugu is most chemically similar to CI chondrites[2,3].

The spectral properties of returned Ryugu samples allow, for the first time, detailed and direct comparison between laboratory spectra of pristine carbonaceous chondrite material with remotely acquired reflectance data of the known parent asteroid surface. Such comparisons can provide important insight into how Vis-NIR spectral features of other primitive small bodies in the Solar System may be better interpreted in terms of surface composition and physical properties. Lab reflectance spectra of bulk and powder Ryugu samples were measured[3] to obtain the average mineralogical and physicochemical properties of material from both collection sites. These spectra exhibit low reflectance values and few absorptions, with the exception of diagnostic phyllosilicate- and carbonate-related features in the NIR and mid-infrared (MIR) range[3].

These results are broadly consistent with both ONC-T and NIRS3 data, though some spectral differences do exist. Detailed analyses of the returned samples indicate that the materials are mineralogically rather homogeneous at the footprint size scale of the reflectance measurements. Thus, the materials on Ryugu's uppermost surface observed by the spacecraft and the majority of samples recovered from Ryugu are thought to have different conditions dominated by non-mineralogical factors. In this study we investigate how porosity-, grain-size-, and space-weathering-dependent variations affect Vis-NIR spectra of carbonaceous chondrites and evaluate the degree to which such factors may influence spectral characteristics of Ryugu's surface. Instead of CI chondrites, we use Murchison CM chondrite, because required sample amount was too much for CI chondrites, only a limited number of fragments arrived to the Earth so far, however, ~5.6 g in total to be required for all experiments in this study. Mineralogy and physical properties of CM and CI chondrites are most similar to Ryugu captured samples than any other carbonaceous chondrites; CM has phyllosilicate-rich (CI > 80 vol.% and Murchison 84 vol.%[12,13]) and anhydrous-silicate-poor mineralogy[14], higher carbon content (CI 4.3–5.4 wt.%, CM 2.2–4.1 wt.%, in contrast to CV, CO, CK 0.1–1.5 wt.%[15]), low bulk density (CI 2110 kg m^{-3}, CM 2200 kg m^{-3}, CO and CV 3030 kg m^{-3}, CK 2900 kg m^{-3} [16,17]), and similar reflectance spectral features (Supplementary Fig. 1a, b and Supplementary Table 1).

We present spectral reflectance data for samples of Murchison with different porosity and grain size and explore how these physical traits influence spectral properties at Vis-NIR wavelengths relevant to Hayabusa2. Effects of space weathering are also evaluated based on results from space weathering simulation experiments of Murchison samples, simulating micrometeoroid bombardments[18,19]. Layered silicates in CM exhibit decomposition temperatures nearly identical to those of CI[20] and thus dehydration behavior by micrometeoroid impact heating is similar between CM and CI. Integrating these experimental results with lab and spacecraft spectra of Ryugu's surface materials provides new insight and context for interpreting telescopic data of other C-class asteroids, allowing for improved interpretation of the relationship between carbonaceous chondrites and primitive asteroids.

Results

Laboratory and remotely-acquired spectra of Ryugu surface materials. As shown in previous studies, ONC-T data in seven bands (wavelength for each band: ul: 0.40 μm, b: 0.48 μm, v: 0.55 μm, Na: 0.59 μm, w: 0.70 μm, x: 0.86 μm, p: 0.95 μm;[21] Supplementary Table 2) acquired over the surface of Ryugu exhibit dark and flat Vis spectra with only subtle variations (~1.5–3% at 0.55 μm for absolute reflectance; ~−0.1–0.3 μm^{-1} between 0.55 to 0.86 μm for spectral slope; Figs. 1a, c and 2) that are correlated with topographical features[6,7,22]. The Hayabusa2 laser altimeter (LIDAR) data also show homogeneous and low normal albedo at 1.064 μm in the −40° to +20° latitude range[23]. Spectral analysis[24] found spectrally blue (decreasing slope with increasing wavelength in the Vis portion of the spectrum) regions inside several small craters, which show bluer (<0.075 μm^{-1} decreasing) spectra for b-x slope (between 0.48 to 0.86 μm in wavelength). Relative to the global average spectral properties of Ryugu, the topographically higher equatorial ridge and the polar regions were also bluer relative to the topographically lower and spectrally redder mid-latitude regions along with the previous mass movement from the equatorial ridge to mid-latitude regions[7,24]. These observations were interpreted to indicate that bluer regions had experienced less space weathering and/or were more recently exposed[6,24,25]. Since both TD1 and TD2 sites are located at the equatorial ridge, collected Ryugu samples are estimated to retain a fresher state of Ryugu component materials.

Lab Vis spectra of Ryugu samples show low reflectance (typically ~1.4–3.4% at 0.55 μm; Fig. 2) and a slight red slope (typically ~0.0–0.6 μm^{-1} between 0.55 to 0.86 μm; Fig. 2), that are generally consistent with ONC-T data as reported[3]. Comparing ONC-T data, TD1 site exhibited brighter spectra compared to TD2 site, consistent with the lab sample Vis spectra[3] (Fig. 1c). Moreover, compared with ONC-T data, lab Ryugu samples show redder (lab Ryugu average: 0.24 ± 0.21 μm^{-1} vs. ONC-T median: 0.13 ± 0.03 μm^{-1} in slope) and brighter (lab Ryugu average: 2.4 ± 0.8% vs. ONC-T median: 2.0 ± 0.1% reflectance at 0.55 μm) spectra (Fig. 2).

NIRS3 data ranging from 1.8 to 3.2 μm in wavelength with an 18-nm spectral resolution[26] (Supplementary Table 2) indicated that the Ryugu surface materials are globally homogeneous showing low NIR reflectance with a weak red slope and constant OH absorption centered at 2.72 μm that is consistent with structural water in phyllosilicates[8]. Lab NIR spectra of Ryugu samples are also broadly consistent with NIRS3 data[8,21] and

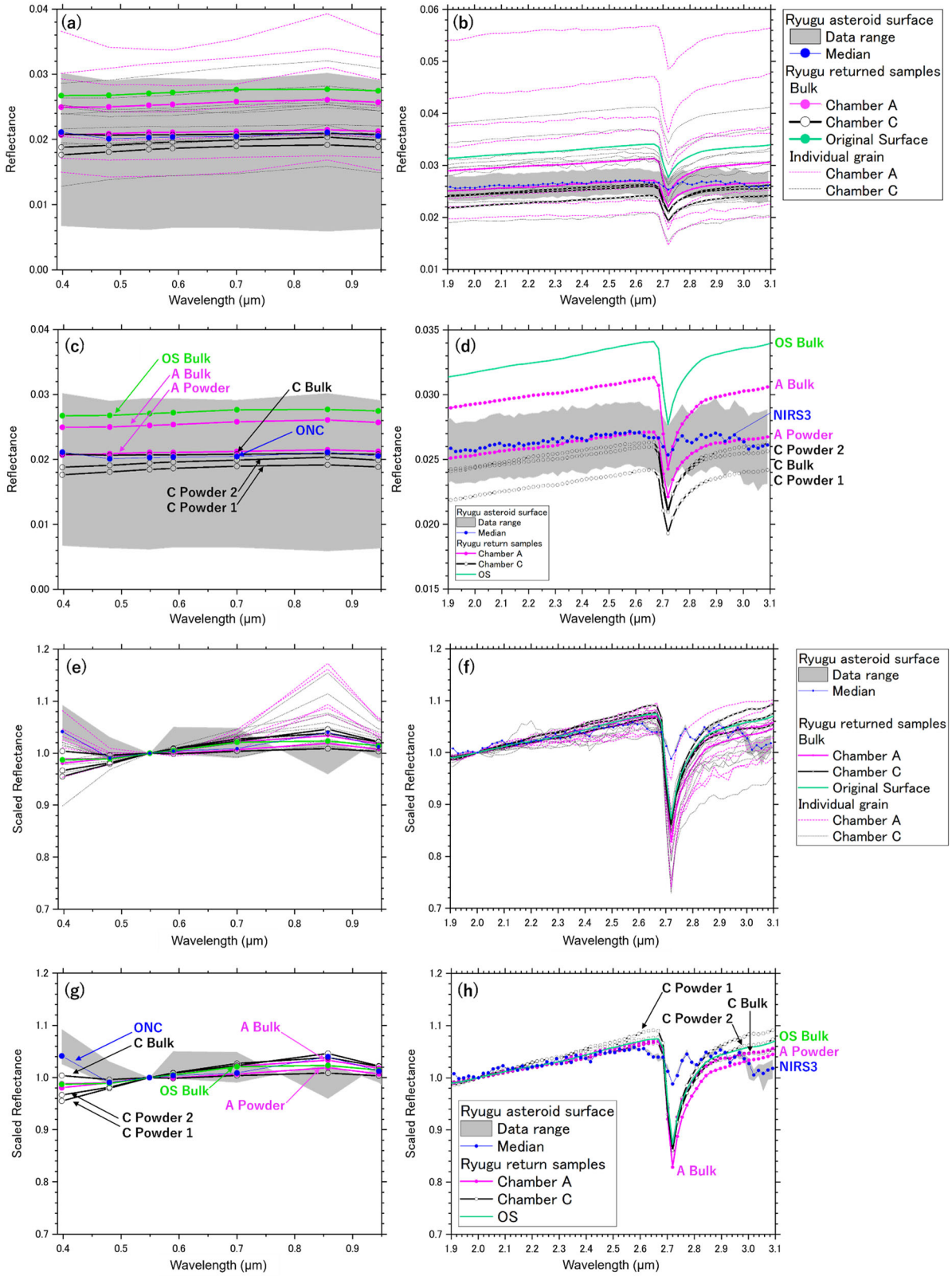

exhibit low reflectance (~2–3%), little variation in spectral shape, and an absorption band at 2.72 μm (Figs. 1b, d and 3a, b). However, the samples are in a different condition: unsorted powder (Chamber A/C Powder), individual grains, and bulk samples as a portion of multiple individual grains (Chamber A/C or OS Bulk)[3,27].

For precise comparison between Ryugu surface spectra and Ryugu sample spectra, we converted Ryugu sample spectra to the spectral resolution of ONC-T and NIRS3 (Supplementary Table 2), because these onboard apparatuses have lower wavelength resolution and the ONC-T have only seven bands with large band widths for each. The converted lab Ryugu sample spectra still

Fig. 1 Lab-measured and remote-sensed Ryugu spectra. Vis (**a**) and NIR (**b**) spectra of Ryugu samples of Chamber A (magenta lines; samples collected at TD1 site), Chamber C (black lines; samples collected at TD2 site), and original surface samples (green lines), and ONC-T and NIRS3 data obtained on 3 September 2018, and on 23 August 2018 and 4–5 September 2018, respectively (gray areas with blue lines as a median). Bulk sample spectra are similar to ONC-T and NIRS3 spectra (**c**, **d**). The spectrum of A0064 with the flat surface is much brighter (>0.05 in reflectance over the entire wavelength range) than the other data and is not displayed here. The same spectra are normalized at 0.55 and 2.0 μm, respectively (**e**–**h**). Ryugu samples shown are: A0026, A0055, A0063, A0064, A0067, A0094, A powder, A bulk, C0002, C0023, C0025, C0040, C0046, C0055, C0076, C0103, C powder 1, C powder 2, C bulk, and OS bulk. A bulk is composed of A0026, A0055, A0058, A0063, A0064, A0067, and A0094, C bulk is composed of C0023, C0025, C0033, C0040, C0061, C0076, and C0103, and OS bulk is composed of A0064, A0067, A0094, C0025, C0033, C0061, C0076, and C0103, respectively. All samples measured for spectra were subsequently analyzed for mineralogy and the results indicate that most of the samples measured for spectroscopy show almost identical mineralogy (Major lithology defined in ref. [3]).

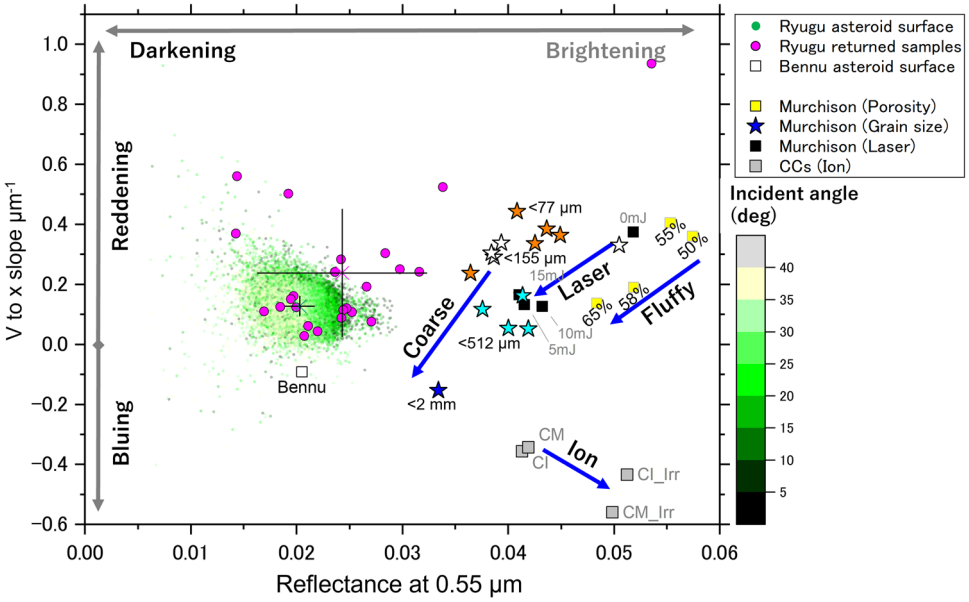

Fig. 2 Comparison of Vis spectral parameters within Ryugu, Bennu, and carbonaceous chondrite samples. Spectral data of Ryugu samples (magenta circles with a standard deviation (1σ)); Murchison CM with the different porosity (yellow squares); Murchison with the different grain size (colored stars; blue for <2 mm, light blue for <512 μm, white for <155 μm, and orange for <77 μm in diameter. Numbers indicate the surface porosity); laser-irradiated Murchison[19] (black squares); lab ion-irradiated C chondrite samples[29] (gray squares). Ryugu asteroid surface data were obtained by ONC-T in latitude 30°N to 30°S on 3 September 2018 (colored circles with a median and quartile deviation). ONC-T data, the phase angles were all close to 30°, but still show a slight variation likely related to the incident angle condition. V to x slope was calculated by dividing the difference between the reflectance at the v band (0.55 μm) and x band (0.86 μm) by the wavelength width. Bennu asteroid surface datum was obtained by OVIRS (white square; data from Dr. Simon, A.).

exhibit similar Vis and NIR spectral properties to those obtained by both ONC-T and NIRS3. Most of the Ryugu sample spectra presented here show a range in absolute reflectance value from ~1.5 to 4% over the entire Vis-NIR, a range that encompasses the median spectra of ONC-T and NIRS3, with a red slope from ~0.4 to ~2.65 μm (Figs. 1, 2, and 3b). The averaged sample spectra, i.e., for Chamber C bulk, Chamber A powder, and Chamber C powder samples, respectively, are within the reflectance value range of the ONC-T data. The general similarity between lab spectra of Ryugu materials and remote NIRS3 observations[8,21] (Fig. 3b) confirms that the returned samples are representative of the materials exposed at Ryugu's surface[10]. However, several notable differences exist between returned sample and ONC-T/NIRS3 spectral data. First, the bulk/powder sample spectra display a 2.72-μm OH band depth value of ~20%, which is much deeper than the ~6% band depth seen in the thermally corrected NIRS3 data (Fig. 3a). Second, lab spectra of individual particles show greater variation in reflectance compared with ONC-T/NIRS3 data, ranging ~1.5–5.5% in Vis and ~2–4% in NIR range[27] (Fig. 1a, b). Laboratory spectra of relevant carbonaceous chondrite materials were analyzed to assess possible origins for these spectral differences further.

Murchison spectra with porosity and grain size variations. Powdered samples of the Murchison CM chondrite were prepared to explore how differences in porosity and grain size influence Vis-NIR spectral properties and for comparison with Ryugu data. How the porosity and grain size were changed is described in detail in Section 5.2.1. Briefly, porosity was varied by tapping the loaded sample dishes (designated Tap-N, where N represents a number of times tapped) or pressing the material into the sample dish. The surface texture was varied by scraping the top of a pressed sample and subsequently sieving additional particulate CM material onto the surface, resulting in a fine-grained dusty and highly porous surface overlying a compacted sample. The samples' porosity was determined by using high resolution CT images (Supplementary Fig. 2). We found that porosity varies between the top and bottom of the powder and thus porosity of the surface layer (definition is described in detail in Supplementary Note 1) is applied in this study (Supplementary Fig. 3). For grain-size effects on spectra, we prepared a single Murchison chip and crushed it to different grain sizes (< 2 mm, <512, <155, and <77 μm in size). At each grain size, spectrum was taken and then the sample was further crushed; all spectra were taken from the same Murchison sample. As for the effects of space weathering, the spectra of Murchison from

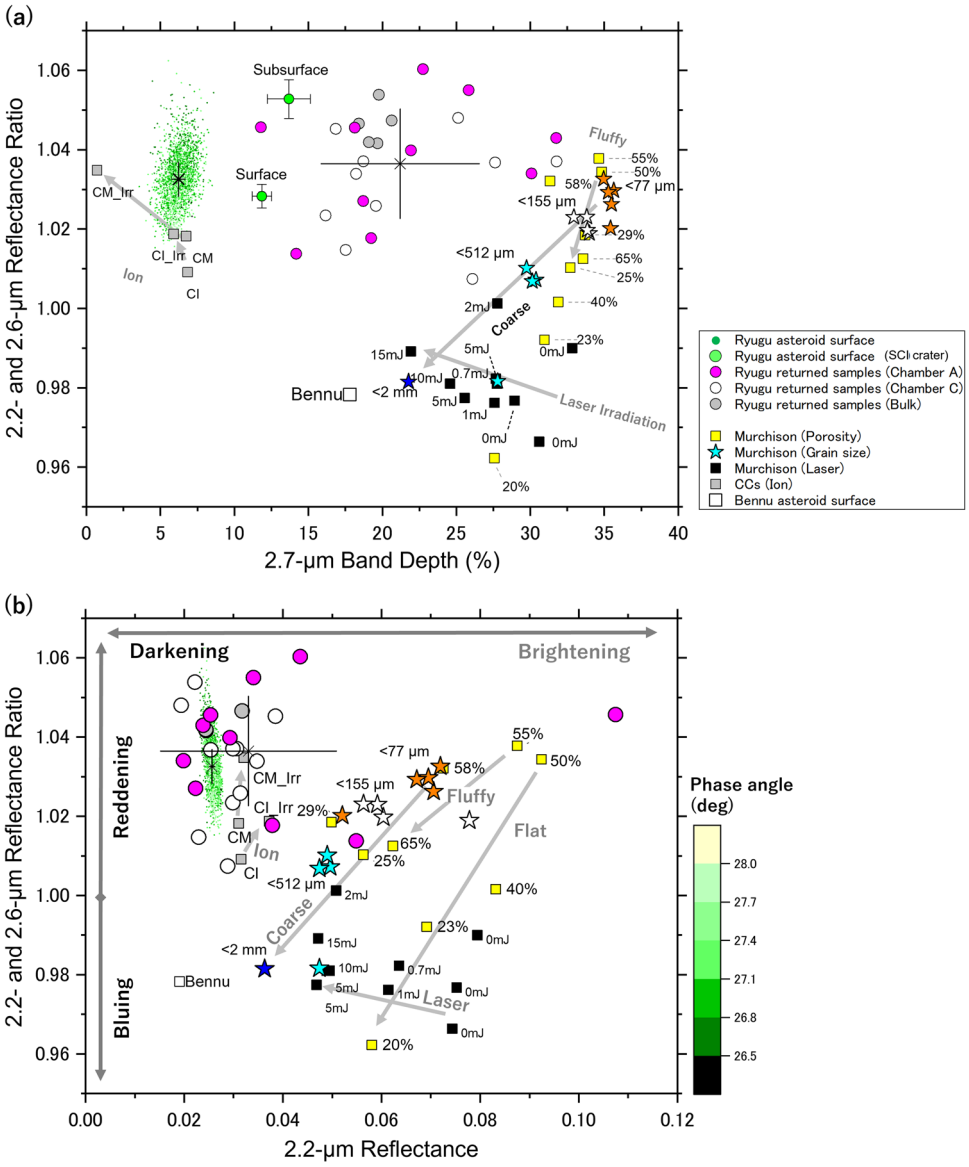

Fig. 3 Comparison of NIR spectral parameters within Ryugu, Bennu, and carbonaceous chondrite samples. The relationship between the NIR reflectance and NIR color (Ratio of 2.6-μm reflectance/2.2-μm reflectance) (**a**), and between the 2.72-μm band depth and NIR color (**b**) of lab Ryugu individual particles[28] (white and magenta circles with a standard deviation (1σ)) and bulk/powder samples[3] (gray circles), lab laser-irradiated Murchison samples[19] (black squares), lab Murchison samples with different porosity (yellow squares), lab ion-irradiated C chondrite samples[29] (gray squares), Ryugu asteroid surface data were obtained by NIRS3 (dots with a median and quartile deviation), along with scaled reflectance data of Ryugu Subsurface, where NIRS3 observed across to the SCI crater, and Surface, outer the SCI crater for the reference 37 (data with a standard deviation (1σ)). Bennu asteroid surface datum was obtained by OVIRS (white square; data from Dr. Simon, A.). For number labels for Murchison samples with different porosity, Tap-0, 10, 20, 40, Hand-press, Press-500 kg, Scraped, Light-airfall, and Heavier-airfall are for 65%, 58%, 55%, 50%, 40%, 20%, 23%, 25%, and 29%, respectively. Due to data availability, ratio of 2.4-μm reflectance/ 2.2-μm reflectance and that of 2.5-μm reflectance/ 2.2-μm reflectance were used for lab ion-irradiated C chondrite samples and lab laser-irradiated Murchison samples, respectively.

experimentally induced space weathering experiments were gathered from previous studies[18,19,28]. Figures 2, 3a, b, and 4a–c show the spectral trends of these integrated Murchison data as functions of physical structure (porosity and grain size) and simulated space weathering. Samples Tap-0, 10, 20, and 40 represent porosities of 65%, 58%, 55%, and 50%, respectively (see Supplementary Fig. 4c), and a decrease in porosity leads to an increase in Vis and NIR reflectances as well as Vis and NIR spectral reddening (increase in spectral slope). In contrast, a strong spectral bluing is produced when the sample surface is pressed, either by hand or machine (Figs. 3a, b and 4a–c), and this effect is only partially reversed when the pressed surface is scraped (see data for Scraped, Hand-press, and Press-500 kg in Fig. 4a–c). With the addition of thicker and thicker dust layers on the sample surface, from Scraped to Light-airfall to Heavier-airfall, the Murchison NIR spectrum becomes as dark and red as that of Tap-0. This indicates that when a thin (<1 mm; Supplementary Fig. 2) powder layer covers an otherwise hard (rocky) surface, the spectral properties are dominated by the fine powder coating and may contain little if any spectral information of the underlying material (e.g., Fig. 3a, b), which is an important piece of information for the interpretation of remote sensing data. In contrast, porosity variations do not significantly affect on the depth and peak position of the 2.7-μm absorption band (Fig. 4a, c) due to an OH stretching mode of structural water

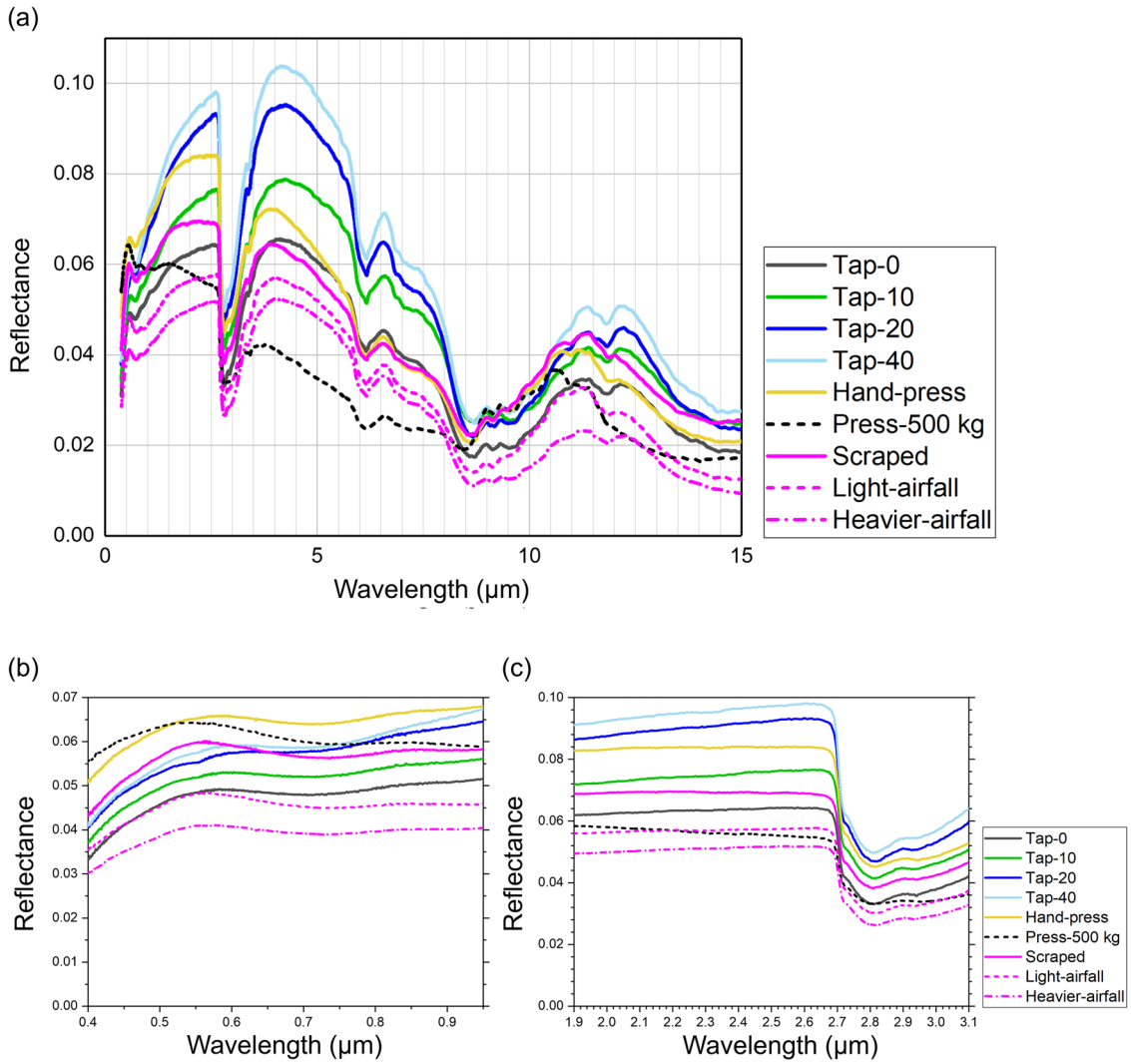

Fig. 4 Reflectance spectra of Murchison affected by porosity and surface condition. The Vis-NIR-MIR (**a**), Vis (**b**), and NIR (**c**) spectra of the Tap-0, 10, 20, and 40, Scraped, Light-Airfall, and Heavier-Airfall Murchison samples.

in phyllosilicates. An exception is the Press-500 kg spectrum that exhibits a distinct decrease of the 2.7-μm band depth. Similar to trends for decreasing porosity, a decrease in grain size also leads to Vis-NIR spectra becoming brighter and redder with no OH-band peak shift (Figs. 2 and 3a, b). A decrease in grain size significantly results in deeper 2.7-μm absorption band depth (Fig. 3a) in contrast with porosity not effective for the band depth. More detailed descriptions are provided in Supplementary Note 1.

Discussion

The Vis-NIR reflectance values, spectral slope, and structural-water absorption position are generally consistent among spectra of the bulk/powder samples from both Chambers A and C. They are also in good agreement with the remotely-sensed data of Ryugu surface (Figs. 2 and 3b). This supports that returned samples have generally homogeneous mineralogy and are representative of Ryugu's surface materials[1,11].

Some lab Ryugu sample data exhibit a slight shift from the ONC-T data in Figs. 1a, e and 2. Bright and spectrally red lab sample spectra contrast with dark and spectrally blue asteroid surface spectra. Figure 2 shows that the physical structures of the grains control the variations among Ryugu sample spectra and ONC-T data. The brightening and reddening trend of Ryugu sample data from the ONC-T data, similar to trends of porosity/compaction, grain size-dependence, and laser-irradiation shown in the Murchison data, suggest the asteroid surface may be more porous and/or coarser-grained, and/or more space weathered than the captured Ryugu samples. These factors may also explain spectral variations observed at NIR wavelengths within the lab data (Fig. 3b). Thus, spectral slope and reflectance cannot determine whether porosity, grain size, or space weathering is responsible for the observed spectral differences. The difference in physical structure of grains may be in part due to the Hayabusa2 sampling processes that shot 5-gram tantalum projectiles into the surface[29] and small carry-on impactor (SCI) experiment that shot a 2-kilogram copper projectile to produce a crater artificially on the surface[9]: Ryugu rocks were broken into multiple fragments because of low physical strength[3] and fresher, less-space-weathered surfaces were exposed. Thus, the remotely-sensed surface spectra are bluer and darker than the lab Vis spectra of the Ryugu samples.

We are aware that several laser irradiation experiments using Murchison CM have been previously performed so far, and both spectral bluing we discuss here and reddening have been reported (e.g., reviewed by ref. [30]). It is indicated that experimental conditions can be effective for spectral response: for spectral reddening after laser irradiation on a Murchison sample[31], their laser pulse had a 0.5−1 microsecond duration[32], which was too long to

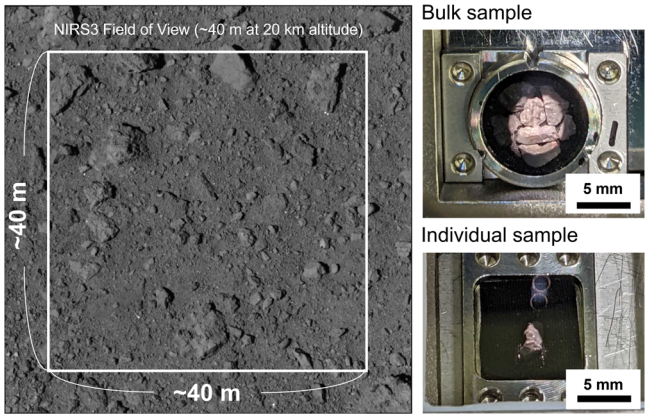

Fig. 5 Field-of-view difference of remote observations and lab measurements. The footprint size images of NIRS3 observations from the Hayabusa2 home position at 20 km altitude (hyb2_onc_20190516_011850_tvf_l2c.fit), and of laboratory measurements using Ryugu bulk samples and individual particles. The contrast and brightness are adjusted.

reproduce micrometeoroid bombardments as pointed[33]. Longer pulse duration[31] was possibly effective for stronger thermal alteration compared to the nano-second pulsed-laser irradiation cases, especially more processed dehydration, therefore, resulting in spectral reddening. The other reported spectral reddening[34], whose sample was 1500-psi pressed pellet samples of Murchison. Pulsed laser heating contributes to produce microscopic bumpy structures due to melting and deposition at the uppermost surface[19]. Then a flat surface condition of the starting material leads drastic surface roughness increasing when spectral change mainly affected by surface roughness due to laser heating.

Note that sample measurement conditions do not perfectly mimic the spacecraft observation conditions, which can also explain the spectral darkening of ONC-T data compared to lab Ryugu spectra. On Ryugu, compared to the lab measurement condition, undisturbed surface grains distributed more randomly were observed by the larger footprint size (~cm–m scale for ONC-T observations vs. ~mm scale for lab measurements; Fig. 5), then reflection condition cannot be as efficient as lab settings and grain shadow areas can be larger and make the reflectance lower.

The 2.72-μm OH absorption band depth of the lab-measured and remote-sensed Ryugu data are clearly different (Fig. 3a), although spectral slope and reflectance values are similar in the NIR range. Pre-launch measurements for calibration of NIRS3 detectors demonstrated that OH absorption strengths in NIRS3 spectra of hydrous carbonaceous chondrites were highly consistent with independent FT-IR reflectance data[35]. This indicates that the shallower absorption band at 2.72-μm in the NIRS3 data compared to the lab spectra of Ryugu samples is not an artifact of instrument response.

Possible causes for the observed weaker OH band in the NIRS3 data are (a) space weathering + porosity/compaction/grain size differences, and (b) all other unignorable effects. (a) Enhanced space weathering effects can produce shallower band depths with only slight spectral reddening (Fig. 3a), and we interpret space weathering to be the dominant cause for the shallower 2.72-μm band observed in NIRS3 data. This is consistent with the NIRS3 observation that spectra of fresher sub-surface materials exposed by the SCI experiment, which produced a ~1.7-m depth crater[9], showed a deeper 2.72-μm band[36,37] (15% increasing compared with Surface and Subsurface in Fig. 3a). To explain the consistent slope between the NIRS3 and lab Ryugu sample data, an additional effect contributing to spectral bluing at NIR wavelengths is required. As shown in Fig. 3a, b, increasing porosity, grain size, and surface roughness effectively induce bluer spectral slopes. Therefore, a space-weathered surface with higher porosity, larger grains, or flatter surfaces relative to the returned sample surfaces on Ryugu can simultaneously explain the differences in the OH band depth and the similarity in other properties between NIRS3 and lab Ryugu spectra. Note that if only porosity/compaction and grain size without space weathering effects are different between Ryugu surface and lab Ryugu samples, the OH band depth, reflectance and spectral slope should change together (e.g., Murchison data in Fig. 3a), which is inconsistent because only a significant difference in band depth is observed.

Second, thermal alteration effects as unignorable effects, i.e., solar radiation and/or decay of the short-lived radiogenic nuclides such as ^{26}Al, could contribute to the OH-band weakening as a result of hydrous mineral decomposition and amorphization[38,39]. In this case, the Ryugu surface material and returned samples should have experienced the same heating events and show the same OH-band depth, which is contrary to what is observed. This is consistent with noble gas analysis confirmed captured Ryugu grains have not experienced higher than 100 °C[2]. Thus, (b) cannot adequately explain the observed spectral mismatch in the OH band depth between the remotely-sensed spectra of Ryugu's surface and the spectra of the returned samples.

This interpretation of the presence and differences in degree of space weathering is also consistent with the Hayabusa2 initial sample analysis results[40], which reported that 6–7% of the small (<~100 μm in size) analyzed grains ($n > 800$) from TD1 and TD2 sites contain an amorphous rim made by solar-wind irradiation, and 1–2% of the grains exhibit evidence for melting and dehydration by micrometeoroid bombardments in the ~1 μm surface layer, exhibiting textures similar to laser-irradiated Murchison CM chondrite samples[19,40]. These small grains are likely the result of the fragmentation of larger grains induced by the sample collection process, consistent with larger population of finer grains compared with surface condition of Ryugu[11], and estimated particle size distributed on Ryugu surface is ~10-mm order based on thermal inertia given by the Thermal Infrared Imager (TIR) observations[41–43]. Therefore, the real ratios of space-weathered grains are higher than that observed in crushed and recovered samples. It is consistent with the possibility of larger grain size contribution on Ryugu's remote-sensed data discussed above.

Space weathering degree of Ryugu in space can be estimated by the cosmogenic exposure age because spallation reactions induced by galactic cosmic rays occur only upper ~1m-depth layer (hereinafter upper-1m layer) of asteroids. Thus, the cosmogenic exposure age suggests the residence time of individual grains to stay in the upper-1m layer. Concentrations of the cosmogenic noble gases such as ^{3}He and ^{21}Ne indicate an exposure age of several million years for Ryugu grains from both Chambers A and C[44]. Consistently, cosmogenic ^{10}Be and ^{26}Al show the exposure age of both Chambers A and C grains is estimated to be on the order of 10^6 years[45]. Furthermore, the cosmogenic ^{21}Ne concentrations are similar among Ryugu samples, suggesting the materials in the upper-1m layer of Ryugu have been constantly mixed probably by impact gardening for $\sim 5 \times 10^6$ years since Ryugu transferred to its current orbit at 1.19 au[4]. The constant mixing in the upper-1m layer is consistent with remote sensing observation of Ryugu surface; the Ryugu surface age is on the order of 10^6 years based on the density of small craters[6]. On the other hand, solar-wind-derived ^{20}Ne concentrations in individual Ryugu grains indicate the residence time at the very surface of the asteroid, which is in general much shorter than the residence time at the upper-1m layer[4], being consistent with continuous mixing of Ryugu regolith.

During the recent ~5×10^6 years, two distinct space weathering processes have occurred in parallel at the surface of Ryugu: solar-wind implantation and micrometeoroid bombardments. The solar-wind implantation effect has proceeded rapidly and has been likely saturated (<10^3 years for the lunar surface[46]; ~10^3 to ~10^4 years for serpentines[47]). In contrast, the micrometeoroid bombardment effect processes more gradually and is expected to continue to alter Ryugu's surface after the solar-wind implantation effect has reached saturation. Micrometeoroid bombardment causes impact heating at the surface of asteroids and promotes mineralogical and spectroscopic alteration. Nanosecond-order pulse laser irradiation experiments have been performed to simulate the heating effects on the asteroid surfaces[18,19,33]. After laser irradiation, hydrous carbonaceous chondrite samples exhibit amorphization, dehydration, and melting of hydrous silicates[19] that are similar to Ryugu grain textures related to space weathering[40].

We concluded that the main cause of spectral alteration, i.e., 2.72-μm OH band weakening with bluing and darkening, on Ryugu can be micrometeoroid bombardments, which have an effective period two-order longer than that of solar-wind implantation and continuously promote dehydration of hydrous silicates at the surface. We estimate ~5×10^6-year space weathering on Ryugu can decrease the 2.72-μm OH band to ~12% at most (See Supplementary Note 2). Note that the estimation gives the upper limit for the micrometeoroid-bombardment duration on Ryugu because upper-1m layer materials are gardened and stay shorter than ~5×10^6 years at the uppermost surface of Ryugu. Thermal fatigue can also contribute to slow the space weathering process on Ryugu. Asteroid Bennu showed cracks and flakes caused by thermal fatigue effects[48] driven by thermal fatigue effects: hydrous chondrites easily produce cracks due to heat cycle than anhydrous chondrites[49]. As well as Bennu, Ryugu is enriched in hydrous silicates, thus such surface resurfacing process can be promoted as suggested[30]. Recent work has reported that multiple Ryugu samples from Chamber A exhibit a weaker 2.72-μm OH band[50], possibly resulting from enhanced space weathering; thus further sample analyses are required.

Compared with Ryugu, the near-Earth S-type asteroid (25143) Itokawa with a semi-major axis of 1.32 au has a similar orbit and thus a common surface environment, i.e., galactic cosmic ray exposure, solar-wind implantation, micrometeoroid impact rates, and regolith gardening effects. The cosmic exposure ages of the upper ~1-m-depth layer of Itokawa were found to be <8×10^6 and 1.5×10^6 years, based on concentrations of cosmogenic noble gases in returned samples[51,52], respectively, which is of comparable order to Ryugu's estimated cosmic-ray exposure ages[4,24,44,45]. The crater age of Itokawa is in good agreement with that of Ryugu; for Itokawa, 3–33×10^6 years is estimated as the crater retention age[53], and for Ryugu, on the order of 10^6 and 10^7 years based on the density of small craters[6] and the artificial crater formation experiment analysis[9], respectively. The solar-wind implantation on Itokawa is considered to be saturated on timescales on the order of 10^3 years[54], comparable to that on Ryugu.

In contrast to Ryugu, however, Itokawa showed a clear dichotomy in spectral properties, more space-weathered dark and red terrain and fresh bright and blue terrain with a large spectral variation acquired by the Hayabusa spacecraft: reflectance exhibits >30% variation at 0.55 μm[55] (~1.5% variation for Ryugu, Fig. 2) and difference between 16.4% and 18.2% at 1.7 μm[56] (2.6 ± 0.05% at 2.2 μm for Ryugu, Fig. 2), Vis slope varies from 1.45 to 1.30 as the reflectance ratio at 0.76 μm/0.41 μm[57] (1.04 ± 0.01 as the reflectance ratio at 0.86 μm/0.55 μm for Ryugu, Fig. 1a, e), NIR slope as ratios of reflectance at 1.54 μm/0.76 μm is 1.33 and 1.20[58] (1.03 ± 0.004 as the reflectance ratio at 2.6 μm/2.2 μm for Ryugu, Fig. 2), and anhydrous silicate 1-μm band depths are 29% and 32.5%[56] (6.2 ± 0.5% for Ryugu, Fig. 3a).

Then, the different surface spectral trends of heterogeneous Itokawa and homogeneous Ryugu can indicate that the space weathering on S-type asteroids alters the surface more slowly compared to that on Cb-type asteroids, which previous laboratory studies can support. The major component of asteroid Itokawa is well-crystalline anhydrous silicates[59,60], whose temperature stability and material strength are higher than those of porous hydrous silicates as the main component of Ryugu:[3] e.g., Mg olivine, e.g., Fa = 28.4 ± 1.2 as the average composition of Itokawa dust particles, is stable up to ~1300 °C[61], and saponite and serpentine decompose at 700 °C and 600 °C, respectively[20]. Hardness values of the Itokawa and Ryugu grains are 8.01–13.01 GPa and 0.18 GPa, respectively[3,62]. Therefore, the surface of Itokawa is more resistant to alteration by micrometeoroid bombardments. It may explain the inferred differences in degree and rate of space weathering due to micrometeoroid bombardments between hydrous and anhydrous near-Earth asteroids, supported by lab space weathering simulation experiments; using olivine samples, the 30-mJ pulsed laser irradiation (equivalent to 10^8-year space weathering) produced little change of band depth at 1 μm[33]. Even multiple (up to 99 times) laser irradiation using olivine samples only had a ~30% decrease in band depth[63]. In contrast, the OH band decreased by 35% by only the 15-mJ laser irradiation onto Murchison[18]. It suggests that, when regolith mass movement and/or impact gardening occur on Itokawa, the exposed area is able to preserve the fresh surface due to micrometeoroid bombardments that results in little mineralogical alteration. Thus, the binary variation of Itokawa spectra could be shown by more space-weathered stable area and relatively fresh exposed area. Regolith resurfacing processes[53,64], as an additional factor for the space weathering process, can reduce the accumulation of space weathering effects for materials exposed at the uppermost surface. However, they are commonly effective on Itokawa and Ryugu, and do not contribute to the different spectral trends between Itokawa and Ryugu.

A B-type asteroid, (101955) Bennu was explored in detail by NASA's the Origins, Spectral Interpretation, Resource Identification, and Security–Regolith Explorer (OSIRIS-REx) spacecraft, and surface reflectance spectra were obtained by the visible-infrared spectrometer OVIRS[65,66]. Based on the observed maximum OH absorption position of ~2.74 μm, and low reflectance of 4.4 ± 0.2%, the surface materials on Bennu are predicted to be similar to the heavily aqueously altered CM or CI or ungrouped C1 chondrites[65–68]. If Bennu is composed of a CM-like material, Bennu would possibly be enriched in chondrules compared to Ryugu, which includes very few and small chondrules[69] similar to the chondrule-free composition of CI chondrites. Vis-NIR spectra of mm-size (the coarsest sample) Murchison samples are the closest match to Bennu's average spectrum (Figs. 2 and 3a, b). This suggests the surface regolith of Bennu consists of coarser grains and/or higher porosity compared with Ryugu, consistent with the previous results[70]. Spectral analysis on Bennu's craters indicated that spectral darkening, bluing, and the 2.7-μm band weakening due to space weathering[71], which shows the consistent trend with spectral changes of laser-irradiated Murchison samples[18,19]. Bluing on Bennu caused by space weathering is also consistent with the equatorial ridge, estimated to be the oldest surface of Bennu[72], showing a redder spectrum[30]. Besides, in contrast to Ryugu, Bennu shows spectral variations related to its surface texture covered by boulders, some of which have possibly survived since Bennu's parent body era[73]. The surface of Bennu is classified by two characteristic textures[74]. The Rugged Unit is more boulder-rich, and more active to get fresh surface[74,75]. The Smooth Unit on Bennu, in contrast, has an older age than the

Rugged Unit (~2×10^6 years vs. ~5×10^5 years[74]), can well retain space-weathered effects on Bennu, processing spectral bluing[30]. The boulders on Bennu have diverse porosity (24–38% for bright boulders vs. 49–55% for dark boulders[76]). Some boulders contain anhydrous silicates[73]. It is suggested that a possible ancient impactor of ordinary-chondrite-like material on Bennu estimated to have been a 36–40 m body in size, at present remaining as the exogenic boulders on Bennu[77]. The sample collection was successfully performed at Hokioi crater, where a fresh region located in the Smooth Unit[74]. The detailed mineralogical properties and its relationship with spectral/physical properties of surface materials on Bennu will be revealed in the near future by samples returned by OSIRIS-REx in 2023, which unveil the space weathering effects on B-type asteroids and its differences and similarities between Bennu and Ryugu.

When integrated with previous reports[4,24,40], our results indicate the alteration history of Ryugu's equatorial region is consistent with the following scenario: Ryugu's parent asteroid formed beyond the CO_2 and H_2O snowlines at heliocentric distance >3–4 au[3]. On the order of 10^8 years ago, Ryugu was formed through the catastrophic collision and disruption of the parent body, e.g., the parent bodies of Polana or Eulalia families[6,78]. The surface regolith materials showing redder spectra have been moving from the equatorial ridge to the higher latitude regions, thus exposing fresh bluer materials in the equatorial region[24]. On the order of 10^5–10^6 years ago, Ryugu might have arrived at the current orbit. Solar-wind implantation dominated the regolith processing and spectral reddening, producing alteration of grain surfaces (at submicron-scale depth) through amorphization and dehydration of hydrous silicates, growth of void structures, and formation of nanophase Fe-rich inclusions within the amorphous silicates[79]. After <10^4 years, solar-wind implantation effects saturated and micrometeoroid bombardment promoting spectral bluing and the OH band decreasing has since been the major space weathering contributor on Ryugu. Due to regolith gardening, the upper-1m layer has been stirred constantly and the uppermost surface has been exposed in turn to micrometeoroid bombardments. Then, the upper-1m layer showed a uniform space-weathering degree. The current spectra of Ryugu's surface as seen remotely are indicative of both saturated solar-wind implantation and ongoing micrometeoroid bombardments.

Conclusions

A comparison of spectral properties between orbital observations of the Cb-type asteroid Ryugu and laboratory measurements of the returned Ryugu samples is presented. The lab spectra of Ryugu samples are similar to the remote-sensed spectra of Ryugu's surface with some notable exceptions: the 2.7-μm band is deeper in Ryugu-sample spectra than Ryugu-surface spectra. Differences in degree of space weathering can readily explain these differences as a primary effect, and porosity and/or grain size are supplementally contributing. Comparing lab spectra of returned samples with spectra acquired by Hayabusa2 during the asteroid encounter suggests (1) only the uppermost surface of Ryugu has been strongly affected by space weathering, (2) some dehydration has likely occurred at the optical surface due to space weathering effects, mainly micrometeoroid bombardments, and (3) the returned Ryugu samples contain a higher proportion of fresh surfaces with lower degrees of space weathering compared with the undisturbed optical surface of Ryugu, because of fragmentation during sample collection. Vis-NIR spectral homogeneity of Ryugu is in contrast to the spectral dichotomy of the S-type asteroid Itokawa. It suggests space weathering may alter Vis-NIR reflectance properties on Cb-type asteroids more rapidly compared with S-type asteroids.

Materials and methods

Data processing of Ryugu lab-measured and remote-sensed spectra. The laboratory measurements of the Ryugu samples were obtained at Tohoku University, Japan, using an FT-IR system (Bruker VERTEX 70v) at standard laboratory conditions (incident, emission, and phase angles of 30, 0, and 30 degrees, respectively) with ~5 nm wavelength resolution[3,27]. In this study, for the precise comparison between FT-IR data with remote-sensing data, the FT-IR data were converted to the data format of the remote-sensing data: wavelength resolution of the FT-IR data was adjusted to both the ONC-T instrument seven band channels (0.40, 0.48, 0.55, 0.59, 0.70, 0.86, and 0.95 μm; Supplementary Table 2)[6,80], and the 18-nm wavelength resolution ranging from 1.8 to 3.2 μm of the NIRS3.

The ONC-T data were obtained on 3 September 2018, of the equatorial region (−30 to +30 degrees in latitude) of Ryugu at ~20 km altitude, which were selected based on the phase angle values close to 30° to be similar to the laboratory standard condition. The raw images were calibrated to the radiance factor (I/F) based on the calibration method[80]. The NIRS3 thermally corrected data, obtained on 23 August 2018 and 4–5 September 2018, around the equatorial region of Ryugu, were selected by also constraining the observations to phase angles close to 30°.

For the NIRS3 spectra, we applied the data correction method[35], using the correction factors for Y 982086, whose reflectance was as low as that of Ryugu. The resultant NIRS3 spectra show slightly higher reflectance with almost similar spectral shape compared with original NIRS3 data[8].

Murchison measurements with different porosity and grain size. The Murchison CM powder sample with grain sizes smaller than 155 μm[35] was scooped and placed in an aluminum sample holder 7 mm in diameter and 3 mm in depth. To produce porosity variations, the packing condition was controlled by tapping on the side of the holder: starting from the sample without tapping (Tap-0), and after tapping 10, 20, and 40 times, referred to as Tap-10, Tap-20, and Tap-40. Thus, Tap-40 was the most compacted sample. Furthermore, we pressed the surface of the Tap-40 sample using a SUS cylinder (by hand for Hand-press and by a pressing machine for 500-kg press), and then produced a diffuse-reflecting surface roughened by a spatula (Scraped). Then, we covered the surface of the Scraped sample with additional Murchison powders sprinkled on the sample surface through a 155-μm mesh filter (Light-/Heavier-airfall): according to the additional powder layer thickness, the condition with the primary surface visible was called Light-airfall, and the condition where the primary surface became totally invisible was called Heavier-airfall. Those processes follow the methods previously described[81,82]. We performed X-ray CT analyses for each porosity case to calculate their porosity (Supplementary Fig. 3 and Supplementary Note 1), and the reflectance spectral measurements. We also used Murchison powder samples sequentially with the following grain size variations: smaller than 2 mm, 512 μm, 155 μm, and 77 μm in size. For each sample, we produced different packing conditions by tapping and each condition's bulk porosity was calculated using the holder volume and sample amount.

The reflectance spectra of each sample were obtained using Bruker VERTEX 70v Fourier-transform infrared (FT-IR) spectrometer at Tohoku University. The incidence, emission, and phase angles were set to 30, 0, and 30 degrees, respectively, for each porosity and grain-size variation. The measured surface area was ~5 mm in diameter. Spectral data were interpolated in order to adjust to ONC-T and NIRS3 channels, respectively. Details of the measurement settings are described[35].

In order to determine the porosity, three-dimensional X-ray CT images of each Murchison sample were obtained using a Comscantecno ScanXmate-D180RSS270 at the Tohoku University Museum operated at 200 kV and 200 μA. The projection number was set to 3000 (0.12° per projection) and the resolution was 5.163 μm per pixel. First, we defined the average porosity of Tap-0, as the maximum value of the surface porosity, calculated from the sample amount of 84.51 mg, a density of 2.31 g cm^{-3} [16], and the volume of the sample holder. Then, the porosity of Tap-10, 20, and 40 was each relatively defined based on the value of Tap-0. In this process, the thickness for each sample condition was determined by the cross-section image stacking: starting from the sample surface, which is defined as the 4% of the cross-sectional surface being occupied with powder grains, reaching at the bottom, with overlayed cross-sectional images first showing filled almost 100% by powder grains. Each calculation was performed using Molcer Plus 3D image software (White Rabbit Corp.) and ImageJ software[83]. Bulk porosity for each sample condition and the various grain-size Murchison samples was calculated using the volume and amount of the sample placed in the holder. See also Supplementary Note 1 for detail.

Data availability

The datasets used and/or analyzed during the current study available at DARTS (https://data.darts.isas.jaxa.jp/pub/hayabusa2/paper/sample/Matsuoka_2023/).

Received: 17 April 2023; Accepted: 5 September 2023;
Published online: 27 September 2023

References

1. Tachibana, S. et al. Pebbles and sand on asteroid (162173) Ryugu: In situ observation and particles returned to Earth. *Science* **375**, 1011–1016 (2022).
2. Yokoyama, T. et al. Samples returned from the asteroid Ryugu are similar to Ivuna-type carbonaceous meteorites. *Science* **379**, eabn7850 (2022).
3. Nakamura, T. et al. Formation and evolution of carbonaceous asteroid Ryugu: Direct evidence from returned samples. *Science* **379**, eabn8671 (2022).
4. Okazaki, R. et al. Noble gases and nitrogen in samples of asteroid Ryugu record its volatile sources and recent surface evolution. *Science* **379**, eabo0431 (2022).
5. Ishiguro, M. et al. Optical properties of (162173) 1999 JU3: In preparation for the JAXA *Hayabusa 2* sample return mission. *Astrophys. J.* **792**, 74 (2014).
6. Sugita, S. et al. The geomorphology, color, and thermal properties of Ryugu: Implications for parent-body processes. *Science* **364**, 1–19 (2019).
7. Tatsumi, E. et al. Global photometric properties of (162173) Ryugu. *Astron. Astrophys.* **639**, A83 (2020).
8. Kitazato, K. et al. The surface composition of asteroid 162173 Ryugu from Hayabusa2 near-infrared spectroscopy. *Science* **7432**, eaav7432–275 (2019).
9. Arakawa, M. et al. An artificial impact on the asteroid (162173) Ryugu formed a crater in the gravity-dominated regime. *Science* **368**, 1–5 (2020).
10. Pilorget, C. et al. First compositional analysis of Ryugu samples by the MicrOmega hyperspectral microscope. *Nat. Astron.* **6**, 221–225 (2022).
11. Yada, T. et al. Preliminary analysis of the Hayabusa2 samples returned from C-type asteroid Ryugu. *Nat. Astron.* **6**, 214–220 (2022).
12. King, A. J., Schofield, P. F., Howard, K. T. & Russell, S. S. Modal mineralogy of CI and CI-like chondrites by X-ray diffraction. *Geochim. Cosmochim. Acta* **165**, 148–160 (2015).
13. Bland, P. A., Cressey, G. & Menzies, O. N. Modal mineralogy of carbonaceous chondrites by X-ray diffraction and Mössbauer spectroscopy. *Meteorit. Planet. Sci.* **39**, 3–16 (2004).
14. Zolensky, M. E. et al. Mineralogy and composition of matrix and chondrule rims in carbonaceous chondrites. *Geochim. Cosmochim. Acta* **57**, 3123–3148 (1993).
15. Pearson, V. K., Sephton, M. A., Franchi, I. A., Gibson, J. M. & Gilmour, I. Carbon and nitrogen in carbonaceous chondrites: elemental abundances and stable isotopic compisitions. *Meteorit. Planet. Sci.* **41**, 1899–1918 (2006).
16. Macke, R. J., Consolmagno, G. J. & Britt, D. T. Density, porosity, and magnetic susceptibility of carbonaceous chondrites. *Meteorit. Planet. Sci.* **46**, 1842–1862 (2011).
17. Britt, D. T. & Consolmagno, S. J. G. J. Stony meteorite porosities and densities: a review of the data through 2001. *Meteorit. Planet. Sci.* **38**, 1161–1180 (2003).
18. Matsuoka, M. et al. Pulse-laser irradiation experiments of Murchison CM2 chondrite for reproducing space weathering on C-type asteroids. *Icarus* **254**, 135–143 (2015).
19. Matsuoka, M., Nakamura, T., Hiroi, T., Okumura, S. & Sasaki, S. Space weathering simulation with low-energy laser irradiation of murchison CM chondrite for reproducing micrometeoroid bombardments on C-type asteroids. *Astrophys. J.* **890**, L23 (2020).
20. Nozaki, W., Nakamura, T. & Noguchi, T. Bulk mineralogical changes of hydrous micrometeorites during heating in the upper atmosphere at temperatures below 1000°C. *Meteorit. Planet. Sci.* **41**, 1095–1114 (2006).
21. Barucci, M. A. et al. Multivariable statistical analysis of spectrophotometry and spectra of (162173) Ryugu as observed by JAXA Hayabusa2 mission. *Astron. Astrophys.* **629**, A13 (2019).
22. Yokota, Y. et al. Opposition observations of 162173 Ryugu: Normal albedo map highlights variations in regolith characteristics. *Planet. Sci. J.* **2**, 177 (2021).
23. Yamada, R. et al. Derivation of 1.064 μm normal albedos on the C-type asteroid Ryugu from laser pulse intensity measurement of the Hayabusa2 LIDAR. *Earth Planets Sp.* **74**, 166 (2022).
24. Morota, T. et al. Sample collection from asteroid (162173) Ryugu by Hayabusa2: Implications for surface evolution. *Science* **368**, 654–659 (2020).
25. Tatsumi, E. et al. Spectrally blue hydrated parent body of asteroid (162173) Ryugu. *Nat. Commun.* **12**, 5837 (2021).
26. Iwata, T. et al. NIRS3: the near infrared spectrometer on Hayabusa2. *Space Sci. Rev.* **208**, 317–337 (2017).
27. Amano, K. et al. Visible-IR spectroscopic diversity of Ryugu coarse grains and comparison to spectral properties of carbonaceous chondrites. *Annual Meeting of the Meteoritical Society*, No. 6166 (2022).
28. Lantz, C. et al. Ion irradiation of carbonaceous chondrites: a new view of space weathering on primitive asteroids. *Icarus* **285**, 43–57 (2017).
29. Sawada, H. et al. Hayabusa2 sampler: collection of asteroidal surface material. *Sp. Sci. Rev.* **208**, 81–106 (2017).
30. Clark, B. E. et al. Overview of the search for signs of space weathering on the low-albedo asteroid (101955) Bennu. *Icarus* **400**, 115563 (2023).
31. Moroz, L. et al. Optical alteration of complex organics induced by ion irradiation: 1. Laboratory experiments suggest unusual space weathering trend. *Icarus* **170**, 214–228 (2004).
32. Moroz, L. V., Fisenko, A. V., Semjonova, L. F., Pieters, C. M. & Korotaeva, N. N. Optical effects of regolith processes on S-asteroids as simulated by laser shots on ordinary chondrite and other mafic materials. *Icarus* **122**, 366–382 (1996).
33. Yamada, M. et al. Simulation of space weathering of planet-forming materials: Nanosecond pulse laser irradiation and proton implantation on olivine and pyroxene samples. *Earth Planets Sp.* **51**, 1255–1265 (1999).
34. Prince, B. S. & Loeffler, M. J. Space weathering of the 3-μm phyllosilicate feature induced by pulsed laser irradiation. *Icarus* **372**, 114736 (2022).
35. Matsuoka, M. et al. An evaluation method of reflectance spectra to be obtained by Hayabusa2 Near-Infrared Spectrometer (NIRS3) based on laboratory measurements of carbonaceous chondrites. *Earth Planets* Sp. **69**, 120 (2017).
36. Galiano, A. et al. Characterization of the Ryugu surface by means of the variability of the near-infrared spectral slope in NIRS3 data. *Icarus* **351**, 113959 (2020).
37. Kitazato, K. et al. Thermally altered subsurface material of asteroid (162173) Ryugu. *Nat. Astron.* **5**, 246–250 (2021).
38. King, A. J., Schofield, P. F. & Russell, S. S. Thermal alteration of CM carbonaceous chondrites: mineralogical changes and metamorphic temperatures. *Geochim. Cosmochim. Acta* **298**, 167–190 (2021).
39. Matsuoka, M. et al. Spectral and mineralogical alteration process of naturally-heated CM and CY chondrites. *Geochim. Cosmochim. Acta* **316**, 150–167 (2022).
40. Noguchi, T. et al. A dehydrated space-weathered skin cloaking the hydrated interior of Ryugu. *Nat. Astron.* **7**, 170–181 (2023).
41. Wada, K. et al. Asteroid Ryugu before the Hayabusa2 encounter. *Prog. Earth Planet. Sci.* **5**, 82 (2018).
42. Shimaki, Y. et al. Thermophysical properties of the surface of asteroid 162173 Ryugu: Infrared observations and thermal inertia mapping. *Icarus* **348**, 113835 (2020).
43. Sakatani, N., Ogawa, K., Arakawa, M. & Tanaka, S. Thermal conductivity of lunar regolith simulant JSC-1A under vacuum. *Icarus* **309**, 13–24 (2018).
44. Nagao, K. et al. Noble gases of Hayabusa2 samples returned from the asteroid Ryugu. in *85th Annual Meeting of The Meteoritical Society* (2022).
45. Nishiizumi, K. et al. Neutron capture 36 Cl in Ryugu samples. *Hayabusa Symposium* (2022).
46. Farrell, W. M., Hurley, D. M. & Zimmerman, M. I. Solar wind implantation into lunar regolith: Hydrogen retention in a surface with defects. *Icarus* **255**, 116–126 (2015).

47. Nakauchi, Y. et al. The formation of H_2O and Si-OH by H_2^+ irradiation in major minerals of carbonaceous chondrites. *Icarus* **355**, 114140 (2021).
48. Molaro, J. L. et al. Thermal fatigue as a driving mechanism for activity on asteroid Bennu. *J. Geophys. Res. Planets* **125**, 1–24 (2020).
49. Delbo, M. et al. Thermal fatigue as the origin of regolith on small asteroids. *Nature* **508**, 233–236 (2014).
50. Le Pivert-Jolivet, T. et al. Multi-scale variations of the ~2.7 µm feature in Ryugu samples, observed by MicrOmega. in *Hayabusa Symposium* S32-08 (2022).
51. Meier, M. M. M. et al. Grain from the surface of near-earth asteroid (25143) Itokawa. in *45th Lunar and Planetary Science Conference* 1247 (2014).
52. Nagao, K. et al. Irradiation history of Itokawa regolith material deduced from noble gases in the Hayabusa samples. *Science* **333**, 1128–1131 (2011).
53. Tatsumi, E. & Sugita, S. Cratering efficiency on coarse-grain targets: Implications for the dynamical evolution of asteroid 25143 Itokawa. *Icarus* **300**, 227–248 (2018).
54. Noguchi, T. et al. Space weathered rims found on the surfaces of the Itokawa dust particles. *Meteorit. Planet. Sci.* **49**, 188–214 (2014).
55. Saito, J. et al. Detailed images of asteroid 25143 Itokawa from Hayabusa. *Science* **312**, 1341–1344 (2006).
56. Abe, M. et al. Near-infrared spectral results of asteroid Itokawa from the Hayabusa spacecraft. *Science* **312**, 1334–1338 (2006).
57. Ishiguro, M. et al. Global mapping of the degree of space weathering on asteroid 25143 Itokawa by Hayabusa/AMICA observations. *Meteorit. Planet. Sci.* **42**, 1791–1800 (2007).
58. Hiroi, T. et al. Developing space weathering on the asteroid 25143 Itokawa. *Nature* **443**, 56–58 (2006).
59. Nakamura, T. et al. Mineral chemistry of MUSES-C Regio inferred from analysis of dust particles collected from the first- and second-touchdown sites on asteroid Itokawa. *Meteorit. Planet. Sci.* **49**, 215–227 (2014).
60. Nakamura, T. et al. Itokawa dust particles: a direct link between S-type asteroids and ordinary chondrites. *Science* **333**, 1113–1116 (2011).
61. Bowen, N. L. & Schairer, J. F. The system MgO-FeO-SiO_2. *Am. J. Sci.* **s5-29**, 151–217 (1935).
62. Tanbakouei, S. et al. Mechanical properties of particles from the surface of asteroid 25143 Itokawa. *Astron. Astrophys.* **629**, A119 (2019).
63. Loeffler, M. J., Dukes, C. A., Christoffersen, R. & Baragiola, R. A. Space weathering of silicates simulated by successive laser irradiation: In situ reflectance measurements of Fo_{90}, Fo_{99+}, and SiO_2. *Meteorit. Planet. Sci.* **51**, 261–275 (2016).
64. Takaki, N. et al. Resurfacing processes constrained by crater distribution on Ryugu. *Icarus* **377**, 114911 (2022).
65. Hamilton, V. E. et al. Evidence for widespread hydrated minerals on asteroid (101955) Bennu. *Nat. Astron.* **3**, 332–340 (2019).
66. Lauretta, D. S. et al. The unexpected surface of asteroid (101955) Bennu. *Nature* **568**, 55–60 (2019).
67. Hamilton, V. E. et al. Evidence for limited compositional and particle size variation on asteroid (101955) Bennu from thermal infrared spectroscopy. *Astron. Astrophys.* **650**, 1–13 (2021).
68. Kaplan, H. H. et al. Bright carbonate veins on asteroid (101955) Bennu: Implications for aqueous alteration history. *Science* **370**, eabc3557 (2020).
69. Nakashima, D. et al. Chondrule-like objects and Ca-Al-rich inclusions in Ryugu may potentially be the oldest Solar System materials. *Nat. Commun.* **14**, 1–9 (2023).
70. Cambioni, S. et al. Fine-regolith production on asteroids controlled by rock porosity. *Nature* **598**, 49–52 (2021).
71. Deshapriya, J. D. P. et al. Spectral analysis of craters on (101955) Bennu. *Icarus* **357**, 1–31 (2021).
72. Bierhaus, E. B. et al. Crater population on asteroid (101955) Bennu indicates impact armouring and a young surface. *Nat. Geosci.* **15**, 440–446 (2022).
73. Dellagiustina, D. N. et al. Variations in color and reflectance on the surface of asteroid (101955) Bennu. *Science* **370**, eabc3660 (2020).
74. Jawin, E. R. et al. Global geologic map of asteroid (101955) Bennu indicates heterogeneous resurfacing in the past 500,000 years. *Icarus* **381**, 114992 (2022).
75. Barnouin, O. S. et al. Geologic context of the OSIRIS-REx sample site from high-resolution topography and imaging. *Planet. Sci. J.* **3**, 75 (2022).
76. Rozitis, B. et al. Asteroid (101955) Bennu's weak boulders and thermally anomalous equator. *Sci. Adv.* **6**, eabc3699 (2020).
77. Le Corre, L. et al. Characterization of exogenic boulders on the near-earth asteroid (101955) Bennu from OSIRIS-REx color images. *Planet. Sci. J.* **2**, 114 (2021).
78. Bottke, W. F. et al. In search of the source of asteroid (101955) Bennu: Applications of the stochastic YORP model. *Icarus* **247**, 191–217 (2015).
79. Keller, L. P., Christoffersen, R., Dukes, C. A., Baragiola, R. A. & Rahman, Z. Ion Irradiation Experiments on the Murchison CM2 Carbonaceous Chondrite: Simulating Space Weathering of Primitive Asteroids. *Lunar and Planetary Science Conference* (2015).
80. Tatsumi, E. et al. Updated inflight calibration of Hayabusa2's optical navigation camera (ONC) for scientific observations during the cruise phase. *Icarus* **325**, 153–195 (2019).
81. Cloutis, E. A., Izawa, M. R. M. & Beck, P. Reflectance spectroscopy of chondrites. in *Primitive Meteorites and Asteroids: Physical, Chemical, and Spectroscopic Observations Paving the Way to Exploration* 273–343 (Elsevier, 2018).
82. Applin, D. M. et al. Spectral reflectance "deconstruction" of the Murchison CM2 carbonaceous chondrite and implications for spectroscopic investigations of dark asteroids. *Icarus* **305**, 203–224 (2018).
83. Schneider, C. A., Rasband, W. S. & Eliceiri, K. W. NIH Image to ImageJ: 25 years of image analysis. *Nat. Methods* **9**, 671–675 (2012).

Acknowledgements

We appreciate supports from the Japan Society for the Promotion of Science (JSPS) Core-to-Core Program "International Network of Planetary Sciences", and KAKENHI from JSPS Grant-in-Aid for Scientific Research on Innovative Areas (Aqua Planetology, grant No. JP17H06459). D.D. was supported by NASA through the Hayabusa2 Participating Scientist program (NNX16AL34G) and the SSERVI Toolbox for Research and Exploration program (NNH16ZDA001N). R.B., A.B., C.L., and S.R. were supported by Centre National d'Etudes Spatiales (CNES).

Author contributions

M.M. coordinated coauthor contributions; M.M., E.K., K.A., and T.Nakamura performed lab sample measurements and analyzed and discussed data; M.M., E.T., T.O., T.H., S.S., K.K., T.I., T.M., Y.Y., T.K., R.H., S.K., Y.C., K.Y., H.Sawada, M.H., N.S., M.Y., H.Suzuki, C.H., K.O., and K.S. analyze and discussed ONC-T and NIRS3 data; R.M., D.D., D.T., R.B., and A.B. interpreted and discussed data and contributed to writing; Y.F., O.S., and S.K. performed sample measurements; K.S., S.T., T.Y., M.N., A.N., A.M., K.Y., M.A., T.O., and T.U. prepared Hayabusa2 samples and discussed data; C.L., S.R., H.Y., T.Noguchi, R.O., H.Y., H.N., M.Y., T.S., S.T., F.T., S.N., S.W., and Y.T. discussed data; All authors reviewed the manuscript.

Competing interests

The authors declare no competing interests.

Additional information

Supplementary information The online version contains supplementary material available at https://doi.org/10.1038/s43247-023-00991-3.

Correspondence and requests for materials should be addressed to Moe Matsuoka.

Peer review information *Communications Earth & Environment* thanks Briony Horgan, Bryce Bolin and Benjamin Sharkey for their contribution to the peer review of this work. Primary Handling Editor: Joe Aslin. A peer review file is available.

Reprints and permission information is available at http://www.nature.com/reprints

Publisher's note Springer Nature remains neutral with regard to jurisdictional claims in published maps and institutional affiliations.

[1]Geological Survey of Japan (GSJ), National Institute of Advanced Industrial Science and Technology (AIST), Tsukuba 305-8567, Japan. [2]Department of Earth Science, Tohoku University, Sendai 980-8578, Japan. [3]Instituto de Astrofisica de Canrias, Calle Vía Láctea, 38205 San Cristóbal de La Laguna, Santa Cruz de Tenerife, Spain. [4]Department of Earth and Planetary Science, University of Tokyo, Bunkyo 113-0033, Japan. [5]Japan Atomic Energy Agency, Tokai 319-1195, Japan. [6]Department of Earth, Environmental and Planetary Sciences, Brown University, Providence, RI 02912, USA. [7]Planetary Science Institute, Tucson, AZ 85719, USA. [8]Jacobs, NASA Johnson Space Center, Houston, TX 77058, USA. [9]Institut d'Astrophysique Spatiale, Université Paris-Saclay, CNRS, Orsay 91405, France. [10]LESIA-Observatoire de Paris, Université PSL, CNRS, Université de Paris, Sorbonne Université, 92195 Meudon Principal Cedex, France. [11]Aizu Research Cluster for Space Science, University of Aizu, Aizu-Wakamatsu 965-8580, Japan. [12]Research Center of the Early Universe, University of Tokyo, Bunkyo 113-0033, Japan. [13]Planetary Exploration Research Center, Chiba Institute of Technology, Narashino, Chiba 275-0016, Japan. [14]Tohoku University Museum, Tohoku University, Sendai 980-8578, Japan. [15]Institute of Space and Astronautical Science (ISAS), Japan Aerospace Exploration Agency (JAXA), Sagamihara 252-5210, Japan. [16]The Graduate University for Advanced Studies, SOKENDAI, Hayama 240-0193, Japan. [17]Digital Architecture Research Center, National Institute of Advanced Industrial Science and Technology, Koto 135-0064, Japan. [18]Center for Data Science, Ehime University, Matsuyama 790-8577, Japan. [19]Department of Physics, Rikkyo University, Toshima 171-8501, Japan. [20]Department of Complexity Science and Engineering, University of Tokyo, Kashiwa 277-8561, Japan. [21]Department of Physics, Meiji University, Kawasaki 214-8571, Japan. [22]Department of Planetology, Kobe University, Kobe 657-8501, Japan. [23]Department of Earth and Planetary Sciences, Hokkaido University, Sapporo 060-0810, Japan. [24]Division of Earth and Planetary Sciences, Kyoto University, Kyoto 606-8502, Japan. [25]Department of Earth and Planetary Sciences, Kyushu University, Fukuoka 819-0395, Japan. [26]Department of Earth and Planetary Systems Science, Hiroshima University, Higashi-Hiroshima 739-8526, Japan. [27]Department of Mechanical Engineering, Kanagawa Institute of Technology, Atsugi 243-0292, Japan. [28]Department of Earth and Environmental Sciences, Nagoya University, Nagoya 464-8601, Japan. ✉email: moe.matsuoka@aist.go.jp